General Theory of Amplitude-Modulation Atomic Force Microscopy

Manhee Lee and Wonho Jhe*

School of Physics and Astronomy, Seoul National University, Seoul 151-747, Korea

(Received 10 March 2006; published 19 July 2006)

We present a general analytical theory that enables one to determine accurately the unknown tip-sample interactions from the experimental measurement of the amplitude and phase of the oscillating tip in amplitude-modulation atomic force microscopy (AM-AFM). We apply the method to the known Lennard-Jones-type forces and find excellent agreement with the reconstructed results. AM-AFM, widely used in air and liquid, is now not only an imaging tool but also a quantitative force measurement tool.

DOI: 10.1103/PhysRevLett.97.036104 PACS numbers: 68.37.Ps, 07.79.Lh, 87.64.Dz

Since its invention two decades ago [1], atomic force microscopy (AFM) has been actively developed in several operation modes as an important scanning probe technology. The amplitude-modulation atomic force microscopy (AM-AFM), usually referred to as the tapping-mode AFM, is one of the most widely used modes of AFM operation. With this versatile technique, solid-state surfaces [2,3] as well as various biological samples [4–6] have been well investigated due to its stable performance in air as well as in liquid environment. Beyond the topographic imaging, AM-AFM has also been used to form and manipulate the nanometric water meniscus between the tip and the substrate [7–9], which have been applied to the fabrication of molecular nanostructures [10,11]. In particular, the elasticity of the nanometric ''water wire'' thus produced was measured [9], which was manifested by a very small change of amplitude signal in AM-AFM. However, quantitative analysis could not be made because theoretical tools to determine the tip-sample interactions in AM-AFM have not been well established.

The dynamics of the AFM probe for given tip-sample interactions has been successfully understood by analytical and numerical methods, describing the bistable and hysteretic behavior of the tip in proximity to the surface [6,12,13]. Nonetheless, there does not still exist a complete understanding of the experimental measurements; for example, the inverse problem of how to extract the tip-sample interactions from the measured motion of the probe is not solved yet, which is mainly due to the nonlinearity of the motion. Although frequency-modulation AFM, another dynamic mode of AFM, is theoretically well formulated and is capable to measure the tip-sample interaction quantitatively [14,15], it always operates with a sizable modulation amplitude kept constant even when the tip is closely adjacent to the sample surface, which may cause strong mechanical contact and damage. Therefore, AM-AFM may be especially suitable for quantitative investigation of nanoscale interactions once general and accurate theoretical tools are developed.

In this Letter, we present a rigorous derivation of the general governing equations for the motion of the probe under both conservative and dissipative forces in AM-AFM operation. In particular, the characteristic differential equations describing the interaction forces are obtained, from which the unknown interactions between the tip and sample can be unambiguously determined. We have applied the formalism to the simple Lennard-Jones-type forces and found excellent agreement with the reconstructed results for arbitrary oscillation amplitude.

AM-AFM is a dynamic force microscopy where the probe tip is excited by an external driving force with constant amplitude at a fixed frequency, usually near or on the free resonance frequency. The oscillation amplitude and the phase shift of the tip motion are the observable quantities that reflect the tip-sample interactions. Let us start with the harmonic oscillator equation which describes the motion of the probe tip [6],

$$m\ddot{\xi} + b\dot{\xi} + k\xi = F\cos\omega t + F_{\text{int}}, \tag{1}$$

where m is the effective mass of the probe, b the damping coefficient, k the spring constant, F the amplitude of the driving force, and F_{int} the interaction force exerted on the probe. Note that these constants can be expressed in terms of experimental quantities; $m = k/\omega_0^2$, $b = k/(Q\omega_0)$, and $F = kA_0/Q$, where ω_0, Q, and A_0 are the resonance frequency, quality factor, and free oscillation amplitude, respectively. ξ is the instantaneous position of the tip, which has a fixed end on top of a mechanical actuator at z, as shown in Fig. 1. If we focus on the harmonic motion of the probe, we obtain the solution of the form,

$$\xi(z, t) = \xi_0(z) + A(z)\sin[\omega t + \theta(z)], \tag{2}$$

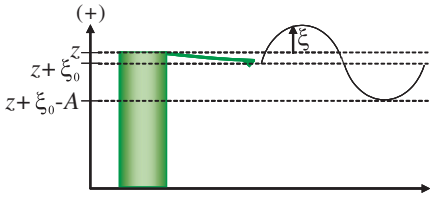

FIG. 1 (color online). Schematic showing the motion of the probe tip.

 © 2006 The American Physical Society

where ξ_0, A, and θ are the mean deflection (<0 in Fig. 1), amplitude, and phase shift of the oscillation, respectively.

In general, F_{int} is a nonlinear function of the tip-sample distance z and contains both conservative and dissipative (i.e., nonconservative) forces,

$$F_{\text{int}} = F_c(z) + F_{\text{nc}}, \tag{3}$$

where the conservative term F_c, by definition, depends only on the distance z. Although it is difficult to find the generalized form of the dissipative force F_{nc}, one can alternatively calculate the dissipation energy, integrated over one period, as

$$\begin{aligned} E_{\text{dis}} &= \int_0^T dt\dot{\xi}F_{\text{nc}} \\ &= \int_0^T dt\dot{\xi}(m\ddot{\xi} + b\dot{\xi} + k\xi - F\cos\omega t - F_c). \end{aligned} \tag{4}$$

Inserting Eq. (2) into Eq. (4), one can obtain the following general dissipation energy,

$$E_{\text{dis}} = -\pi(FA\cos\theta - b\omega A^2), \tag{5}$$

which is equivalent to the previous result obtained by a different approach [16]. Therefore, the dissipated energy, which is always given by Eq. (5), is a general and equivalent description of F_{nc} regardless of its specific form as long as the probe motion is harmonic.

To determine the probe motion analytically, let us consider the following form of interaction,

$$F_{\text{int}} = F_c(z) - \Gamma(z)\dot{z}, \tag{6}$$

where Γ represents the "effective" damping coefficient of a given dissipative interaction. Such a form of force may describe many physically interesting interactions such as the van der Waals, electrostatic, hydrodynamic, or capillary meniscus forces. Note that although the term $-\Gamma(z)\dot{z}$ may be replaced by some other specific forms of dissipation, one may still employ the effective and intuitive coefficient Γ as a parameter describing a given dissipation [15], which will also result in the same formula of dissipation energy, Eq. (5).

Combining Eqs. (1) and (6), one can rewrite the equation of motion as

$$m\ddot{\xi} + b\dot{\xi} + k\xi = F\cos\omega t + F_c(z + \xi) - \Gamma(z + \xi)\dot{\xi}, \tag{7}$$

where $z + \xi$ is the instantaneous tip-sample distance, with z regulated by external feedback control of the actuator. Inserting Eq. (2) into Eq. (7), multiplying both sides of the resulting equation by $\sin(\omega t + \theta)$ and $\cos(\omega t + \theta)$, and then integrating over an oscillation period, one can obtain the two general analytical relations for the amplitude, phase, and interaction forces as

$$\int_0^\pi \frac{d\tau}{\pi} F_c(z + A\cos\tau)\cos\tau = -\frac{F}{2}\sin\theta + \frac{A}{2}(k - m\omega^2), \tag{8}$$

$$\int_0^\pi \frac{d\tau}{\pi} \Gamma(z + A\cos\tau)\sin^2\tau = \frac{1}{2}\left(\frac{F}{A\omega}\cos\theta - b\right). \tag{9}$$

Here we have used the approximation $|\xi_0| \ll |z + A\sin(\omega t + \theta)|$. This condition is satisfied in practice under typical operating conditions [17] and is normally assumed in the analysis of dynamic atomic force microscopy [6,12]. From the governing equations given by Eqs. (8) and (9), the amplitude and phase at a given frequency and distance (that is, the resonance curves at a given distance) are completely determined, provided that F_c and Γ which describe the tip-sample interactions are known.

Conversely, with the amplitude and phase measured at a distance z, one can derive the corresponding interaction forces F_c and Γ that satisfy Eqs. (8) and (9). To invert the integral equations, we formally express F_c and Γ in terms of the Laplace transform of certain functions $C(\lambda)$ and $\gamma(\lambda)$ [15], respectively, as

$$F_c(z) \equiv \int_0^\infty d\lambda e^{-\lambda z} C(\lambda), \tag{10}$$

$$\Gamma(z) \equiv \int_0^\infty d\lambda e^{-\lambda z} \gamma(\lambda). \tag{11}$$

This procedure implicitly requires that the interaction vanishes as $z \to \infty$, which is always satisfied. Substituting Eqs. (10) and (11) into Eqs. (8) and (9), we obtain

$$\int_0^\infty d\lambda C(\lambda) e^{-\lambda z} I_1(\lambda A) = \frac{F}{2}\sin\theta - \frac{A}{2}(k - m\omega^2), \tag{12}$$

$$\int_0^\infty d\lambda \gamma(\lambda) e^{-\lambda z} \frac{I_1(\lambda A)}{\lambda A} = \frac{1}{2}\left(\frac{F}{A\omega}\cos\theta - b\right), \tag{13}$$

where $I_1(\lambda A)$ is the modified Bessel function of the first kind of order one and is represented by the power series,

$$I_1(\lambda A) = \sum_{k=0}^{\infty} \frac{(\lambda A)^{2k+1}}{2^{(2k+1)} k!(k+1)!}. \tag{14}$$

Inserting this into Eqs. (12) and (13), one can finally transform the integral equations of Eqs. (8) and (9) into the following linear differential equations of infinite order that F_c and Γ satisfy

$$\begin{aligned} \sum_{k=0}^{\infty} \frac{A^{2k+1}(z)}{2^{(2k+1)} k!(k+1)!} \frac{d^{2k+1}}{dz^{2k+1}} F_c(z) &= -\frac{F}{2}\sin\theta(z) \\ &+ \frac{A(z)}{2}(k - m\omega^2), \end{aligned} \tag{15}$$

$$\sum_{k=0}^{\infty} \frac{A^{2k}(z)}{2^{(2k+1)}k!(k+1)!} \frac{d^{2k}}{dz^{2k}}\Gamma(z) = \frac{1}{2}\left(\frac{F}{A(z)\omega}\cos\theta(z) - b\right), \tag{16}$$

with the boundary conditions

$$\frac{d^k}{dz^k}F_c(z) = \frac{d^k}{dz^k}\Gamma(z) = 0 \quad \text{as } z \to \infty, \quad k = 0, 1, 2, \ldots. \tag{17}$$

In principle, the tip-sample interactions represented by F_c and Γ can be *exactly* determined by numerical integration of Eqs. (15) and (16). In practice, however, one may consider only the first few order terms until the desired accuracy is reached. This process depends on how many order terms in the series expansion of the derivatives in Eqs. (15) and (16) are kept. We will confirm later that one can always obtain a satisfactory accuracy both (i) for small modulation amplitude, where consideration of only the first term suffices and (ii) for an arbitrary amplitude, where higher-order terms should be included.

Let us consider, for simplicity, the first order term (i.e., $k = 0$ term) in Eqs. (15) and (16). We can easily obtain the following 1st order expressions for the interaction forces in terms of the *known* amplitude and phase,

$$F_c^{(1)}(z) = \int_z^{\infty} dz\left[\frac{F}{A(z)}\sin\theta(z) - (k - m\omega^2)\right], \tag{18}$$

$$\Gamma^{(1)}(z) = \frac{F}{A(z)\omega}\cos\theta(z) - b. \tag{19}$$

Differentiating Eq. (18) with respect to z, the force gradient can be obtained, which is equivalent to the elasticity of any binding material, such as the water meniscus, that exists between the tip and substrate [9]. On the other hand, Eq. (19) can be used to calculate the corresponding dissipation energy by direct integration of $F_{\text{nc}}^{(1)}$ given by $-\Gamma^{(1)}(z)\dot{z}$. Note that Eq. (19) or Eq. (5) implies that if the amplitude A is kept constant by a feedback loop, the simultaneously acquired phase θ provides the information on energy dissipation. That is why phase imaging provides an additional capability of, for example, mapping material domains [6].

To demonstrate the accuracy and validity of the formalism that determines the tip-sample interactions, we first preassume the interaction, evaluate analytically the resulting amplitude change and phase shift from Eqs. (8) and (9), and then reconstruct the tip-sample forces by solving Eqs. (15) and (16). The validity of the theory can then be directly justified by comparing the assumed and the reconstructed forces. For example, let us consider the conservative Lennard-Jones-type force that contains $1/z^6$ (repulsive) and $1/z^2$ (attractive) force terms [15,18],

$$F_{\text{int}}(z) = F_0\left(\frac{l^4}{3z^6} - \frac{1}{z^2}\right), \tag{20}$$

where F_0 is a constant and l is the characteristic distance for which the attractive force is at minimum.

Substituting Eq. (20) into Eqs. (8) and (9) and solving them simultaneously, the amplitude and phase curves for different free oscillation amplitude A_0 are obtained, as in Fig. 2. The coexistence of different solutions gives rise to the hysteresis behaviors [12,19], consisting of two stable states ($\overline{AB}$, $\overline{CD}$) and one bistable sate ($\overline{BD}$). As shown in Fig. 2(a), as the tip is brought close to the surface, the attractive force increases and thus the amplitude decreases through the point A in the lower branch. When the tip approaches the point B, the tip jumps to its upper stable state C. If the tip is pulled off from the surface at this state C, it follows the upper branch, $C \to D \to A$. Note that with the decrease of A_0, the coexistence region gradually disappears, as shown in Figs. 2(a), 2(c), and 2(e). On the other hand, as the tip experiences the repulsive force, the phase shift exhibits a dramatic change, as shown in Figs. 2(b), 2(d), and 2(f). Therefore, measurement of the phase is a very sensitive way to identify the repulsive region.

Now we are able to *reconstruct* the tip-sample interaction forces by inserting the approach curves of Fig. 2 ($\infty \to A \to B \to C \to 0$) into Eq. (15). We have solved Eq. (15) considering only up to the third order terms (i.e., up to $k = 2$ term). Figure 3 presents the preassumed force (solid curve) of Eq. (20) as well as the reconstructed forces (dotted curve) as a function of the distance z for $A_0/l = 1$, 0.8, and 0.1. Note that the 1st order solution corresponds to Eq. (18), whereas the 2nd and the 3rd order solutions are

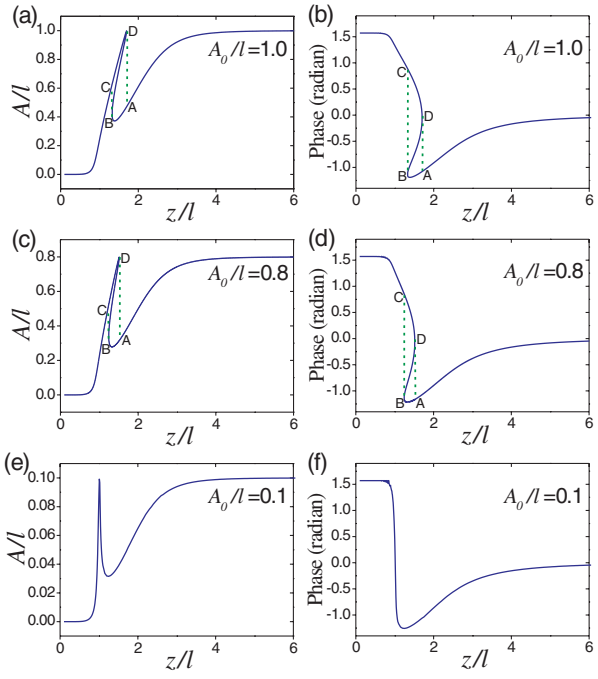

FIG. 2 (color online). Amplitude and phase curves for different free oscillation amplitudes A_0/l, with $F_0Q/(l^3k) = 5$. With the known force of Eq. (20), one can calculate the amplitude and phase responses from the governing Eqs. (8) and (9).

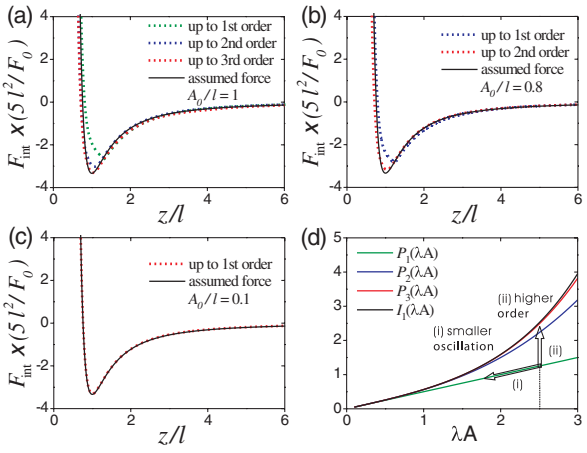

FIG. 3 (color online). (a)–(c) Preassumed (solid curve) and reconstructed (dotted curve) forces for different A_0/l. Here the vertical axis scale factor is $F_0/(5l^2) = 0.3$ nN for $2F_0/(3l^2) = 1$ nN and $l = 1$ nm. (d) Plot of the exact and approximate values of I_1 of Eq. (14).

obtained by numerical integration of the corresponding order terms in Eq. (15). There is an overall agreement between the preassumed and the reconstructed forces in all cases, but some discrepancies exist near $z = l$ where the force curve suddenly reverses its slope. Interestingly, the discrepancy is gradually disappeared and an excellent agreement is obtained, with the decrease of A_0 as well as with the inclusion of the higher-order terms at a given A_0, as shown in Figs. 3(a)–3(c). This is expected, since the accuracy of the reconstructed force is determined by the approximation for $I_1(\lambda A)$ as shown in Fig. 3(d), where P_1, P_2, and P_3 are the polynomials including up to the first, second, and third order terms in the Taylor expansion of $I_1(\lambda A)$, Eq. (14), respectively. As observed in Fig. 3(d), we obtain an excellent agreement as the oscillation amplitude is decreased [case of (i)] or as the higher-order terms are included at a given amplitude [case of (ii)].

Here the discrepancy between the assumed and the reconstructed forces at a given tip-sample distance z is associated with the difference between the values of I_1 and P_i ($i = 1, 2, 3, \ldots$) for a given λA which also depends on z. Therefore, the difference between I_1 and P_i at a given z provides the minimum value of the numerical error. For example, the difference between the assumed and the reconstructed forces, with the terms up to the 3rd (1st) order included, is about 1.1% (42%) at $z/l = 1$ for $A_0/l = 1$ [see Fig. 3(a)], whereas the difference between I_1 and P_3 (P_1) is about 0.5% (37%) at $\lambda A \approx 2$ which is estimated from the integrand of Eq. (10) at $z/l = 1$. Note that the appropriate higher-order terms in Eq. (15) that should be included to obtain a solution with the desired accuracy can be estimated from the fact that $\lambda \sim 1/l$ and $A \sim A_0$ so that $\lambda A \sim A_0/l$. Thus, if $A_0/l = 1$, i.e., $\lambda A \sim 1$, then it is sufficient, from Fig. 3(d), to consider terms only up to the 3rd order in Eq. (15) to obtain the accuracy of about 1%, as shown in Fig. 3(a). Of course, as the higher-order terms are included, the higher accuracy is obtained.

In summary, we have rigorously derived the general governing integral equations, Eqs. (8) and (9), which completely determine the motion of the probe from a known tip-sample interaction. We also have obtained the general differential equations, Eqs. (15) and (16), which allow one to reconstruct the unknown tip-sample interactions from the measured motion of the probe in AM-AFM. The present work will enable one to make a *comprehensive* analysis of the experimental measurement of the amplitude and phase in AM-AFM, which is essential to understand the scan images of sample as well as their physical-chemical properties [20]. AM-AFM is now expected to be widely employed as a quantitative force measurement tool in addition to its atomic-resolution imaging capability.

We are grateful to M.-H. Hong and H. E. Noh for helpful discussions. This work was supported by the CRI Program of Korean Ministry of Science and Technology.

*Corresponding author.
Email address: whjhe@snu.ac.kr

[1] G. Binnig, C. F. Quate, and C. Gerber, Phys. Rev. Lett. **56**, 930 (1986).
[2] W. H. J. Rensen, N. F. van der Hulst, A. G. T. Ruiter, and P. E. West, Appl. Phys. Lett. **75**, 1640 (1999).
[3] Y. Seo, H. Choe, and W. Jhe, Appl. Phys. Lett. **83**, 1860 (2003).
[4] J. K. H. Hörber and M. J. Miles, Science **302**, 1002 (2003).
[5] A. Knoll *et al.*, Nature (London) **3**, 886 (2004).
[6] R. García and R. Perez, Surf. Sci. Rep. **47**, 197 (2002).
[7] L. Zitzler, S. Herminghaus, and F. Mugele, Phys. Rev. B **66**, 155436 (2002).
[8] S. Gomez-Monivas, J. J. Saenz, M. Calleja, and R. García, Phys. Rev. Lett. **91**, 056101 (2003).
[9] H. Choe *et al.*, Phys. Rev. Lett. **95**, 187801 (2005).
[10] M. Cavallini *et al.*, Appl. Phys. Lett. **83**, 5286 (2003).
[11] R. García, M. Tello, J. F. Moulin, and F. Biscarini, Nano Lett. **4**, 1115 (2004).
[12] J. P. Aimé, R. Boisgard, L. Nony, and G. Couturier, Phys. Rev. Lett. **82**, 3388 (1999).
[13] R. García and A. San Paulo, Phys. Rev. B **61**, R13381 (2000).
[14] Franz J. Giessibl, Rev. Mod. Phys. **75**, 949 (2003).
[15] J. E. Sader and S. P. Jarvis, Appl. Phys. Lett. **84**, 1801 (2004); J. E. Sader *et al.*, Nanotechnology **16**, S94 (2005).
[16] B. Anczykowski *et al.*, Appl. Surf. Sci. **140**, 376 (1999).
[17] $\xi_0/(z + A) \approx (F_{int}/k)/(z + FQ/k) \approx 1/Q$, where Q typically exceeds 10^2.
[18] U. Durig, Appl. Phys. Lett. **76**, 1203 (2000).
[19] L. Nony, R. Boisgrad, and J. P. Aimé, J. Chem. Phys. **111**, 1615 (1999).
[20] G. Reiter *et al.*, Phys. Rev. Lett. **87**, 226101 (2001).